International Journal of Computational Science and Engineering Research
ISSN: XXXX- XXXX(Online) , http://www.ijcser.com/
Issue Type: Regular Issue , Vol. 1, Issue. 1, 2024 , Pages: 7 - 13
Received: 04 May 2024 ; Accepted: 20 August 2024 ; Published: 25 September 2024.
Research Paper Type : Research Paper , https://doi.org/10.XXX/XXXX.XXXX.XX.XXXX

Artificial Neural Networks based SMES Implanted Smart Grid for EV Charging Station

M. Rana Prathap [1*], **P. Reddy Sekhar** [2]

[1,2] Department of EEE, Mother Theresa Institute Of Engineering and Technology (A),Palamaner, JNTUA, AP, India

Abstract: The battery life time of an electric vehicle (EV) has significant impact on the development of EV. The proposed converter can operate in a step-up mode and a step-down both with bidirectional power flow control. In addition, the model can independently control power flow between any two low-voltage sources. Artificial Neural Networks (ANN) were used as a closed-loop control structure to control the DC/DC converters in the topology, whilst a rule-based control strategy was used to control the operating states of the hybrid energy storage system. The performance of the ANN controller was also experimentally found to be sufficient when used in conjunction with the rule-based control strategy. In extension we are using ANN controller to generate the triggering pulses. The ANN circuit will be controlling the input and outputs. The system allows one to utilize batteries that are optimized for energy density seeing that the system was able to actively limit the power drawn from the battery, whilst the circuit configuration, operation, steady-state analysis, and closed-loop control of the proposed BDC are discussed according to its three modes of power transfer.

Keywords: Electric Vehicle, Energy storage systems, ANN, Smart Grid, DC-DC converter

1. Introduction

The concept of the Smart grid has offered consumers increased reliability and reduction in total energy losses, and has become a promising alternative for a traditional power distribution system. One area of study for the connection of a Smart grid to the distribution grid is the impact of power quality (PQ) problems on the overall power system performance. These PQ problems include voltage and frequency deviations in the grid voltage and harmonics in the grid voltage and load currents. To overcome the a forementioned PQ problems, several power-conditioning types of equipment such as active filters, uninterruptible power supplies, dynamic voltage restorers, and unified PQ conditioners are usually employed by consumer stop protect their loads and systems against PQ disturbances in the distribution network.

A functional diagram for a typical (FCV/HEV) power system is illustrated in Fig. 1 [4, 13]. The low-voltage FC stack is used as the main power source, and SCs directly connected in parallel with FCs. The dc/dc power converter is used to convert the FC stack voltage into a sufficient dc-bus voltage in the driving inverter for supplying power to the propulsion motor. Furthermore, ES1 with rather higher voltage is used as the main battery storage device for supplying peak power, and ES2 with rather lower voltage could be an auxiliary battery storage device to achieve the vehicle range extender concept [13]. The function of the bidirectional dc/dc converter (BDC) is to interface dual-battery energy storage with the dc-bus of the driving inverter. Generally, the FC stack and battery storage devices have different voltage levels. Several multiport BDCs have been developed to provide specific voltages for loads and control power flow between different sources, thus reducing overall cost, mass, and power consumption [14-27]. These BDCs can be categorized into isolated and no isolated types still has limited static voltage gains, resulting in a narrow voltage range and a low voltage difference between the high-and low-side ports. In isolated converters, high-frequency power transformers are applied to enable galvanic isolation. A few isolated multiport BDC topologies have been investigated, such as the flyback, half- or full-bridge circuits, dual-active bridges, and resonant circuits. The literature suggests that no isolated BDCs are more effective than typical

isolated BDCs in EVs derived no isolated multi-input converter topologies by way of a combination of buck, boost, Ćuk, and Sepic. In the three-port non-isolated multi-input-multi-output (MIMO) converter topologies for interfacing a renewable source, a storage battery, and a load simultaneously. The three double-input converters developed in [19] comprise a single-pole triple-throw switch and only one inductor. A modular non-isolated MIMO converter was presented in [26]. This converter is applied to hybridize clean energy sources of EVs and the basic boost circuit was modified and integrated. However, the voltage gain of the MIMO boost circuit is limited in practice, because of the losses associated with some components such as the main power switch, inductor, filter capacitor, and rectifier diode. To overcome this drawback, three-port power converter that has high-gain characteristic and contains FC, battery sources and stacked output for interfacing HEV, as well as a dc-microgrid was presented [27]. Although the multiport BDC discussed in [25] can interface more than two sources of power and operate at different voltage levels, it still has limited static voltage gains, resulting in a narrow voltage range and a low voltage difference between the high-and low-side ports.

According to this, and after successfully experimenting with schemes based on closed-loop control scheme , the performance of a control for the boost converter based on multilayer neural networks will be evaluated. However, unlike other techniques used previously, the algorithm proposed here evolve both the architecture and the weights in the network (not just their training), in order to find the optimal configuration of the network, and avoid manual techniques to infer the size or the subsequent pruning of the network, ensuring an optimum control architecture that facilitates the performance evaluation.

The network evolution was made using genetic algorithms (GA), which are characterized by using the concepts of natural evolution to find a solution [4], supported on the mechanisms of heredity, mutation and selection. Ref. [5] suggest that evolutionary algorithms are excellent candidates for searches not informed in very complex state spaces, like in the real world, due to the randomness of mutations and the process of "natural" selection allow to avoid local maxims. Also genetic coding and parents crossing allow approaching gradually to the solution.

The developed algorithm was used to design the artificial neural network to control a DC/DC boost converter. This study proposes a new BDC topology for FCV/HEV power systems that consists of an interleaved voltage-doubler structure [9, 28] and a synchronous buck-boost circuit. It features two main operating modes: a low-voltage dual-source-powering mode and a high-voltage dc-bus energy-regenerating mode. In addition, the proposed converter can independently control power flow between any two low-voltage sources when in the low-voltage dual-source buck/boost mode. A similar topology was introduced in [29] that only describes a brief concept. By contrast, this study presents a detailed analysis of the operation and closed-loop control of this new topology as well as simulation and experimental results for all its modes of operation. Moreover, this study expanded the topology presented in [29] because the proposed converter can operate over a wider range of voltage levels. The main characteristics of the proposed converter are summarized as follows:

- interfaces more than two dc sources for different voltage levels,
- controls power flow between the dc bus and the two low-voltage sources and also independently controls power flow between the two low-voltage sources,
- enhances static voltage gain and thus reduces switch voltage stress, and
- possesses a reasonable duty cycle and produces a wide voltage difference between its high- and low-side ports.

2. Literature Survey

SMESMODELING:

There are two classes of SMES model-Current Source Converter (CSC) and Voltage Source Converter (VSC) based on the different connection way of converter. Both converters used to control power exchange between the system and power into the system SMES by independently adjusting its active and reactive. The main requirement of converter in the power transmission system is to control the active and reactive power flow to maintain its system voltage stability. It is achieved by the electronic converter and the electronic convert electrical energy from AC to DC .For VSC, the input voltage is kept constant and output voltage is in dependent of load.

RIPPLEFILTER:

A Low Pass Filter(LPF) is a filter that passes signals with a frequency lower than as elected cut off frequency and attenuates signals with frequencies higher than the cut off frequency. The exact frequency response of the filter depends on the filter design. The filter is sometimes called a high-cut filter or treble-cut filter in audio applications. Alow-pass filter is the complement of a high-pass filter.

Electronic low-pass filters: First order RC Filter:

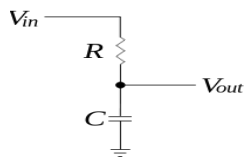

Fig.1. Passive, first order low-pass RC filter.

Parallel with the load. The capacitor exhibits reactance, and block slow-frequency signals, forcing them through the load instead. At higher frequencies the reactance drops, and the capacitor effectively functions as a short circuit.

RL Filter:

A resistor–inductor circuit or RL filter is an electric circuit composed of resistors and inductors driven by a voltage or current source. A first order RL circuit is composed of one resistor and one inductor and is the simplest type of RL circuit. A first order RL circuit is one of the simplest analogue infinite impulse response electronic filters. It consists of a resistor and an inductor, either in series driven by a voltage source or in parallel driven by a current source.

Second order: RLC filter:

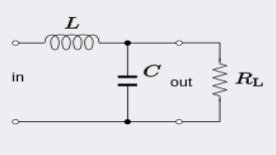

Fig.2. RL Ccircuitasalow-Pass filter.

DC-DCCONVERTERS:

ADC–DC Converter with a high step-up voltage gain is used for many applications such as high intensity discharge lamp ballasts for Automobile head lamps, Fuel Cell Energy Conversion systems, Solar Cell Energy Conversion systems and Battery backup systems for Uninterruptible Power Supplies. Theoretically, a DC–DC Boost Converter can achieve a high step-up voltage gain with an extremely high duty ratio. However, in practice, the step up voltage a in is limited due to the effect of power switches, rectifier diodes and the equivalent series resistance of inductors and capacitors.

a

Operating principle:

The key principle that drives the Boost Converter is the tendency of an inductor to resist changes in current. In a boost converter, the output voltage is always higher than the input voltage. A schematic of a boost power stage is shown in Figure2.11. When the switch is closed, current flows through the inductor, which stores energy from the current in a magnetic field. During this time, the switch acts like a short circuit in parallel with the diode and the load, so no current flows to the right hands ide of the circuit.

TOPOLOGY AND OPERATION MODES

OPERATION MODES

The proposed BDC topology with dual-battery energy storage is illustrated in Fig. 2, where *VH*, *VES*1, and *VES*2 represent the high-voltage dc-bus voltage, the main energy storage (ES1), and the auxiliary energy storage (ES2) of the system, respectively. Two bidirectional power switches (*SES*1 and *SES*2) in the converter structure, are used to switch on or switch off the current loops of ES1 and ES2, respectively. A charge-pump capacitor (*CB*) is integrated as a voltage divider with four active switches (*Q*1, *Q*2, *Q*3, *Q*4) and two-phase inductors (*L*1, *L*2) to improve the static voltage gain between the two low-voltage dual sources (*VES*1, *VES*2) and the high-voltage dc bus (*VH*) in the proposed converter. Furthermore, the additional *CB* reduces the switch voltage stress of active switches and eliminates the need to operate at an extreme duty ratio. Furthermore, the three bidirectional power switches (*S*, *SES*1, *SES*2) displayed in Fig. 2 exhibit four-quadrant operation and are adopted to control the power flow between two low-voltage dual sources (*VES*1, *VES*2) and to block either positive or negative voltage. This bidirectional power switch is implemented via two metal-oxide-semiconductor field-effect transistors (MOSFETs), pointing in opposite directions, in series connection.

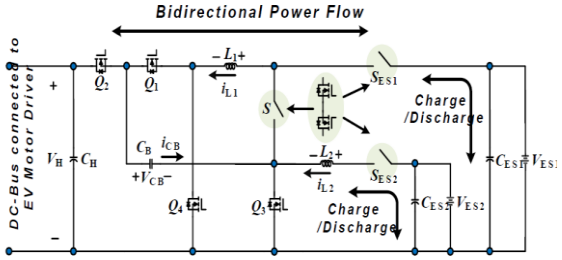

Fig. 3. Proposed BDC topology with dual-battery energy storage.

A. Low-Voltage Dual-Source-Powering Mode

Fig. 3(a) depicts the circuit schematic and steady-state waveforms for the converter under the low-voltage dual-source-powering mode. Therein, the switch *S* is turned off, and the switches (*SES*1, *SES*2) are turned on, and the two low-voltage dual sources (*VES*1, *VES*2) are supplying the energy to the dc-bus and loads. In this mode, the low-side switches *Q*3 and *Q*4 are actively switching at a phase-shift angle of 180°, and the high-side switches *Q*1 and *Q*2 function as the synchronous rectifier (SR). Based on the typical waveforms shown in Fig. 3(b), when the duty ratio is larger than 50%, four circuit states are possible (Fig. 4). In the light of the on/off status of the active switches and the operating principle of the BDC in low-voltage dual-source-powering mode, the operation can be explained briefly as follows.

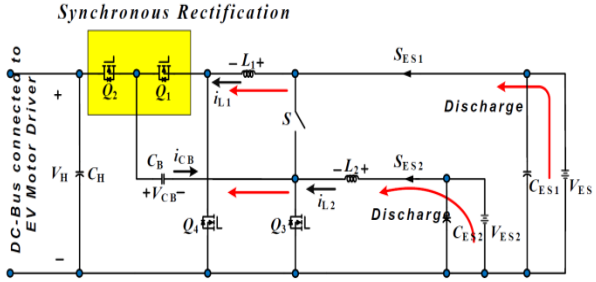

(a)

State 1 [t0 < t < t1]: During this state, the interval time is (1-*Du*)*Tsw*, switches *Q*1, *Q*3 are turned on, and switches *Q*2, *Q*4 are turned off. The voltage across *L*1 is the difference between the low-side voltage *VES*1 and the charge-pump voltage (*V*CB), and hence *iL*1 decreases linearly from the initial value. In addition, inductor *L*2 is charged by the energy source *VES*2, thereby generating a linear increase in the inductor current. The voltages across inductors *L*1 and *L*2 can be denoted as

$$L_1 \frac{di_{L1}}{dt} = V_{ES2} - V_{CB}$$

$$L_2 \frac{di_{L2}}{dt} = V_{ES2}$$

State 2 [t1 < t < t2]: During this state, the interval time is (*Du*-0.5)*Tsw*; switches *Q*3 and *Q*4 are turned on; and switches *Q*1 and *Q*2 are turned off. The low-side voltages *VES*1 and

*VES*2 are located between inductors *L*1 and *L*2, respectively, thereby linearly increasing the inductor currents, and initiating energy to storage. The voltages across inductors *L*1 and *L*2 under state 2 can be denoted as

$$L_1 \frac{di_{L1}}{dt} = V_{ES1}$$
$$L_2 \frac{di_{L2}}{dt} = V_{ES2}$$

State 3 [t2 < t < t3]: During this state, the interval time is (1-*Du*)*Tsw*; switches *Q*1 and *Q*3 are turned on, whereas switches *Q*2 and *Q*4 are turned off. The voltages across inductors *L*1 and *L*2 can be denoted as

$$L_1 \frac{di_{L1}}{dt} = V_{ES1}$$
$$L_2 \frac{di_{L2}}{dt} = V_{CB} + V_{ES2} - V_H$$

State 4 [t3< t <t4]: During this state, the interval time is (*Du*-0.5)*Tsw*; switches *Q*3 and *Q*4 are turned on, and switches *Q*1 and *Q*2 are turned off. The voltages across inductors *L*1 and *L*2 can be denoted as

$$L_1 \frac{di_{L1}}{dt} = V_{ES1} \qquad L_2 \frac{di_{L2}}{dt} = V_{ES2}$$

B. High-Voltage DC-Bus Energy-Regenerating Mode

In this mode, the kinetic energy stored in the motor drive is fed back to the source during regenerative braking operation. The regenerative power can be much higher than what the battery can absorb. Consequently, the excess energy is used to charge the energy storage device. The circuit schematic and the steady-state waveforms of the BDC under the high-voltage dc bus energy-regenerating mode are illustrated in Fig. 5.

Therein, the current in the inductors is controlled by the active switches *Q*1 and *Q*2, which have a phase-shift angle of 180° and thereby direct the flow away from the dc-bus and toward the dual energy storage devices; the switches *Q*3 and *Q*4 function as the SR to improve the conversion efficiency.

On the basis of the steady-state waveforms shown in Fig. 5(b), when the duty ratio is below 50%, four different circuit states are possible, as shown in Fig. 6. In the light of the on-off status of the active switches and the operating principle of the BDC in high-voltage dc-bus energy-regenerating mode, the operation can be depicted briefly as follows.

State 1 [t0 < t < t1]: During this state, the interval time is *DdTsw*; switches *Q*1 and *Q*3 are turned on, and switches *Q*2 and *Q*4 are turned off. The voltage across *L*1 is the difference between the low-side voltage *VES*1 and the charge-pump voltage *VCB*; hence, the inductor current *iL*1 decreases linearly from the initial value. In addition, inductor *L*2 is charged by the energy source *VES*2, which also contributes to the linear increase in the inductor current. The voltages across inductors *L*1 and *L*2 can be denoted as

$$L_1 \frac{di_{L1}}{dt} = V_{ES1} - V_{CB}$$
$$L_2 \frac{di_{L2}}{dt} = V_{ES2}$$

State 2 [t1 < t < t2]: During this state, the interval time is (0.5-*Dd*)*Tsw*; switches *Q*3 and *Q*4 are turned on, and switches *Q*1 and *Q*2 are turned off. The voltages across inductors *L*1 and *L*2 are the positive the low-side voltages *VES*1 and *VES*2, respectively; hence, inductor currents *iL*1 and *iL*2 increase linearly. These voltages can be denoted as

$$L_1 \frac{di_{L1}}{dt} = V_{ES1}$$
$$L_2 \frac{di_{L2}}{dt} = V_{ES2}$$

State 3 [t2 < t < t3]: During this state, the interval time is *DdTsw*; switches *Q*1 and *Q*3 are turned off, and switches *Q*2 and *Q*4 are turned on. The voltage across *L*1 is the positive low-side voltage *VES*1 and hence *iL*1 increases linearly from the initial value. Moreover, the voltage across *L*2 is the difference of the high-side voltage *VH*, the charge-pump voltage *VCB*, and the low-side voltage *VES*2, and its level is negative. The voltages across inductors *L*1 and *L*2 can be denoted as

$$L_1 \frac{di_{L1}}{dt} = V_{ES1}$$
$$L_2 \frac{di_{L2}}{dt} = V_{ES2} + V_{CB} - V_H$$

State 4 [t3 < t < t4]: During this state, the interval time is (0.5-*Dd*)*Tsw*; switches *Q*3 and *Q*4 are turned on, and switches *Q*1 and *Q*2 are turned off. The voltages across inductors *L*1 and *L*2 can be denoted as

$$L_1 \frac{di_{L1}}{dt} = V_{ES1}$$
$$L_2 \frac{di_{L2}}{dt} = V_{ES2}$$

C. Low-Voltage Dual-Source Buck/Boost Mode

The circuit schematic for this mode, which involves the transfer of energy stored in the main energy storage to the auxiliary energy storage and vice versa is presented in Fig. Therein, the topology is converted into a single-leg bidirectional buck-boost converter.

As shown in Fig. when the duty cycle of the active bidirectional switch *S* is controlled, the buck converter channels power from main energy storage to the auxiliary energy storage. By contrast, when the duty cycle of switch *Q*3 is controlled, power flows from the auxiliary energy storage to main energy storage, indicating that the converter is operating in boost mode.

Voltage Gain

The voltage gains of the proposed BDC can be derived by applying the principle of inductor volt-second balance to the different modes. To enhance simplicity and practicality, the equivalent series resistances (ESRs) of the inductors *L*1 and *L*2 have been substituted into the state equations as nonideal cases, and the parameters $R_{L1}=R_{L2}=R_L=50\text{m}\Omega$ are also given.

1) Low-Voltage Dual-Source-Powering Mode

The relationship among the voltage gains of the three dc sources under steady-state operation are given by (17) and (18).

$$\frac{V_H}{V_{s2}} = \left[(k+1) - \frac{2V_{RL}}{V_{s2}}\right]\frac{1}{1-D_u}$$
$$\frac{V_H}{V_{s1}} = \left[\frac{k}{(k+1)} - \frac{2V_{RL}}{V_{s1}}\right]\frac{1}{1-D_u}$$

where *VRL* is the voltage difference across the ESR of inductance, *k* is the ratio of $V_{s1}=V_{ES1}$ to $V_{s2}=V_{ES2}$, and D_u is the duty cycle of Q_3 and Q_4 and is >50%.

Using (17) and (18), the ideal static voltage gains of V_H/V_{s1} and V_H/V_{s2} can be expressed as (19) and (20).

$$\frac{V_H}{V_{s2}} = \frac{k+1}{1-D_u}$$
$$\frac{V_H}{V_{s1}} = \frac{k}{(1-D_u)(k+1)}$$

Accordingly, the relation between dc-bus voltage V_{IH} and the dual-source voltages$(V_{ES1}, V_{ES2})$is given by (21).

$$\frac{V_H}{V_{s1}+V_{s2}} = \frac{1}{1-D_u}\ ; V_{s1} = kV_{s2}$$

2) High-Voltage DC-Bus Energy-Regenerating Mode

Under steady-state operation, the relationship among the voltage gains of the three dc sources are given by

$$\frac{V_{s1}}{V_H} = (D_d - \frac{2V_{RL}}{V_H})\frac{k}{k+1}$$
$$\frac{V_{s2}}{V_H} = (D_d - \frac{2V_{RL}}{V_H})\frac{1}{k+1}$$

where *Dd* is the duty cycle of Q1 and Q2 and is <50%.
From (22) and (23), the ideal static voltage gains of *Vs*1/*VH* and *Vs*2/*VH* are given as (24) and (25).

$$\frac{V_{s1}}{V_H} = \frac{D_d k}{k+1}$$
$$\frac{V_{s2}}{V_H} = \frac{D_d}{k+1}$$

Accordingly, the relation between the dual-source voltages (*VES1*, *VES2*) and the dc-bus voltage *VH* is given by (26).

$$\frac{V_{s1}+V_{s2}}{V_H} = D_d\ ; V_{s1} = kV_{s2}$$

Although these voltage gains are reduced by the ESR of the inductors under the nonideal situation, the parasitic effect is relatively small and thus the reduced voltage gain can be easily compensated for by increasing the duty control.

3) Low-Voltage Dual-Source Buck/Boost Mode

The relation between the two low-side voltages is given by (27).

$$\begin{cases} V_{ES2} - V_{RL2} = D_s V_{ES1}\ ; (buck\ \ mode) \\ V_{ES1} = \dfrac{1}{1-D}(V_{ES2} - V_{RL2})\ ; (boost\ \ mode) \end{cases}$$

In (27), *Ds* is the duty cycle of *S* for the energy transferred from the main energy storage to the auxiliary energy storage, whereas *D* is the duty cycle of *Q*3 for the energy transferred from the auxiliary energy storage to the main energy storage. The relationship between the two low-side voltages without the effect of the ESR of inductors can be expressed as (28).

$$\begin{cases} V_{ES2} = D_s V_{ES1}\ ; (buck\ \ mode) \\ V_{ES1} = \dfrac{V_{ES2}}{1-D}\ ; (boost\ \ mode) \end{cases}$$

B. Charge-Pump Voltage

The voltage across the *CB* under different modes can be derived as follows.

1) Low-Voltage Dual-Source-Powering Mode

$$V_{ES1}D_u + (V_{ES1} - V_{CB})(1-D_u) = 0$$
$$V_{CB} = \frac{V_{ES1}}{(1-D_u)}$$

2) High-Voltage DC-Bus Energy-Regenerating Mode

$$V_{ES1}(1-D_d) + (V_{ES1} - V_{ES2})D_d = 0$$
$$V_{CB} = \frac{V_{ES1}}{D_d}$$

C. Voltage Stresses on Switches

To simplify the voltage stress analyses of the converter, the voltage ripples on the capacitors were ignored. As shown in Figs. 4, 6, 8, and 9, the maximum voltage stresses of the main power MOSFETs *Q*1~*Q*4 can be obtained directly as (33)-(36).

$$V_{Q_1,\max} = V_H$$
$$V_{Q_2,\max} = V_H - V_{CB}$$
$$V_{Q_3,\max} = V_H - V_{CB}$$
$$V_{Q_4,\max} = 2V_{ES1} - V_{CB}$$

D. Characteristic of Uniform Average Current Sharing

Through charge balance principles and the state-space averaging technique, the averaged state equations can be obtained directly as

$$\frac{2(i_{L1} - i_{L2})(1-D_u)}{C_B f_{SW}} = 0$$
$$\frac{2(i_{L1} - i_{L2})D_d}{C_B f_{SW}} = 0$$
$$\frac{(i_{L1} + i_{L2})R_H - V_H}{R_H C_H} = 0$$

where *IH*=*VCH*/*RH*.
From (37)-(39), the following equation can be obtained:

$$i_{L1} = i_{L2} = \frac{i_H}{2}$$

From (40), the uniform average current sharing can be determined, independent of the values of the capacitors.

Artificial Neural Network Controller:

Artificial Neural Networks (ANN) or connection is systems are computing systems that are inspired by, but not identical to, biological neural networks that constitute an Ima brain. Such systems " learn " to perform tasks by considering examples, generally without programmed with task-specific

rules. For example, in image recognition, they might learn to identify images that contain cats by analyzing example images that have been manually labeled as " cat "or" no cat" and using the results to identify cats into their images. They do this without any prior knowledge of cats, for example, that they have fur, tails, whiskers and cat-like faces. Instead, they automatically generate identifying characteristics from the examples that they process.

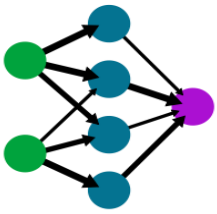

Fig.4. A Simple Neural Network.

MATLAB/SIMULATION

MATLAB is a high-performance language for technical computing. It integrates Computation, visualization, and programming in an easy-to-use environment where problems and solutions are expressed in familiar mathematical notation. Typical uses include Math and computation Algorithm development Data acquisition Modeling, simulation, and prototyping Data analysis, exploration, and visualization Scientific and engineering graphic

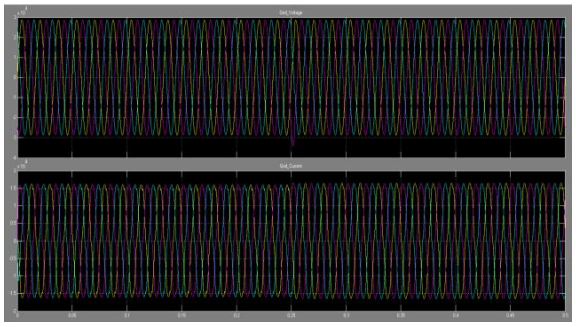

Fig.5. Voltage across the Grid

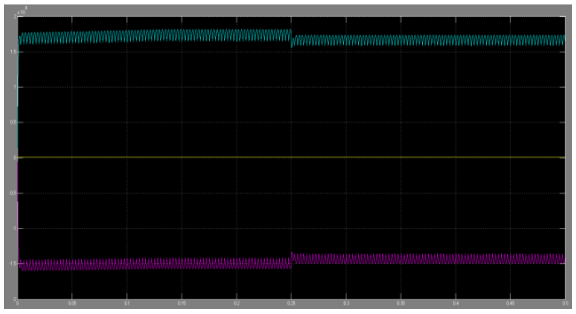

Fig.6. Battery output across the vehicle

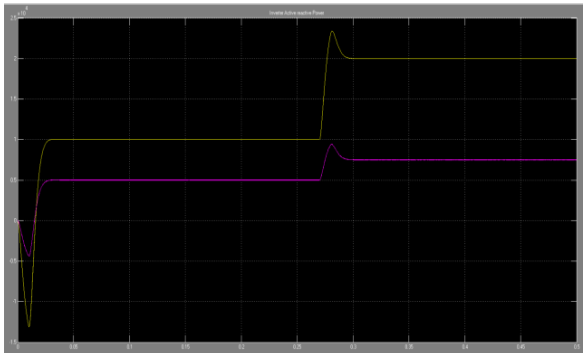

Fig.7. Power quality across the output of inverter

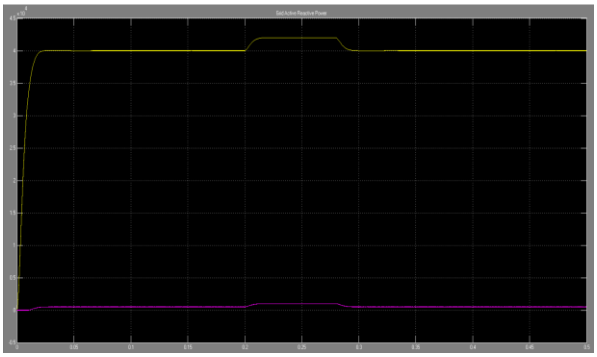

Fig.8. Power quality across the Grid

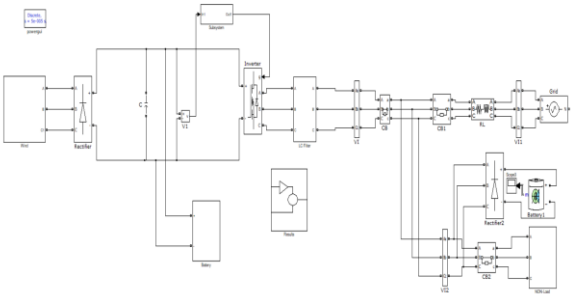

Fig.9. ANN circuit with main circuit.

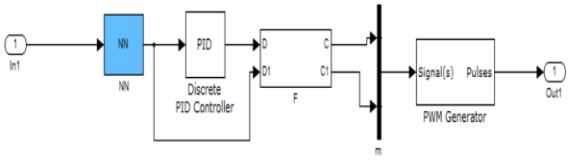

Fig.10. ANN controller circuit in control circuit side

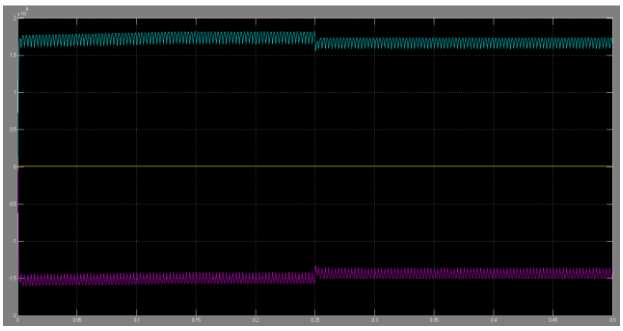

Fig.11. Battery voltage and current at output side

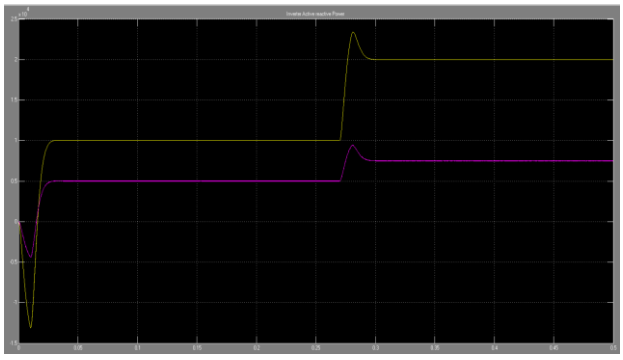

Fig.12. Active and reactive power across the inverter

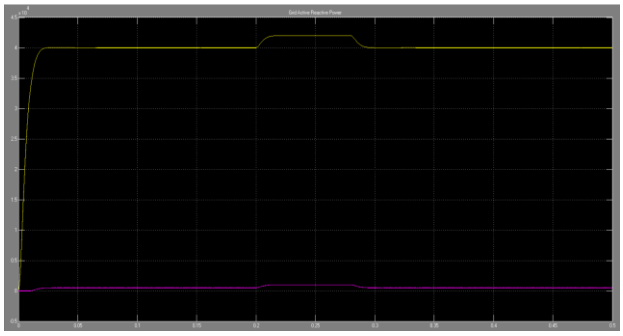

Fig.13. Power quality across the grid.

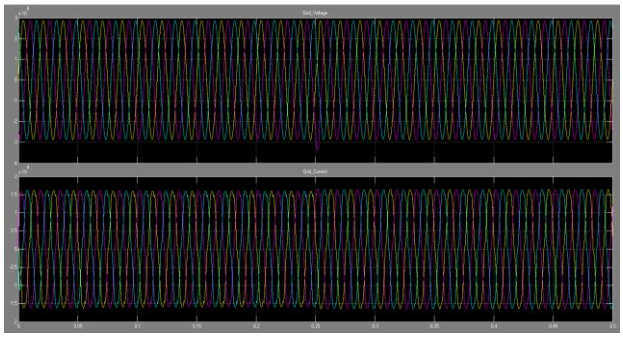

Fig.14. Output across the Grid

6. Conclusion and Future Scope

The effect of using a SMES unit to improve the stability of a power distribution smart grid with EVs has been analyzed. The results obtained show that the use of a SMES unit can smooth the voltage of the EV charging station right after the EVs are connected to the grid. I fault occurs, the SMES unit is able to respond quickly to restore the load terminal voltage by compensating both active and reactive power of the system and improve system transient stability. The application of a SMES unit has also be unconfirmed to be able to effectively compensate the instantaneous voltage dip of the load terminal, stabilize powered is tribute ion networks with EVs, and improve the irpower quality.

References

[1]. K.T.Chau and C.C.Chan,“ Emerging energy-efficient technologies for hybrid electricvehicles, ” Proc.IEEE,vol.95,no.4,pp.821–835,Apr.2007.

[2]. S.P.Richardson,D.Flynn,andA.Keane,“Optimalcharging of electric vehicles in low-voltage distribution systems,”IEEETrans.Power.Syst.,vol.27,no.1,pp.268–279,Feb.2012.

[3]. K.Qian,C.Zhou,M.Allan,andY.Yuan,“Modeling of load demand due to EV battery charging in distribution systems,” IEEE Trans.Power.Syst.,vol.26,no.2,pp.802–810,May2011.

[4]. P.Zhang, K.Qian, C.Zhou, B.G.Stewart, and D.M.Hepburn, “A methodology for optimization of power systems demand due to electric vehicle charging load,” IEEETrans.Power.Syst.,vol.27,no.3,pp.1628–1636,Aug.2012.

[5]. K.Clement-Nyns, E.Haesen, and J.Driesen,“ The impact of charging plug-in hybrid electric vehicles on a residential distribution grid, ” IEEE Trans. PowerSyst.,vol.25,no.1,pp.371–380,Feb.2010.

[6]. J.X.JinandX.Y.Chen,“ Study on the SMES application solutions for smart grid, ”PhysicsProcedia, vol.36, pp.902–907,2012.

[7]. C.A.Luongo,“Super conducting storage systems: An overview, ” IEEETrans.Magn.,vol.31,no.4,pp.2214–2223,Jul.1996.

[8]. S.Kolluri,“Application of distributed super conducting magnetic energy storage system (D-SMES)in the entergy system to improve voltage stability,”in Proc.IEEE PowerEng.Soc.WinterMeet.,2002,vol.2,pp.838–841.

[9]. H.A.Peterson, N.Mohan, and R.W.Boom, “ Superconductive energy storage inductor-converter units for power systems, ” IEEETrans. Power App. Syst.,vol.PAS-94,no.4,pp.1337–1346,Jul.1975.

[10]. M.V.AwareandD.Sutanto, “SMES for protection of distributed critical loads,” IEEE Trans. PowerDel. ,vol.19,no.3,pp.1267–1275,Jul.2004.

[11]. Hareesh Sita, Reddy, P Umapathi Reddy& Kiranmayi, R. (2020). Optimal location and sizing of UPFC for optimal power flow in a deregulated power system using a hybrid algorithm. International Journal of Ambient Energy,.Vol.43, No.1, pp.1413-1419, 2020.

[12]. K. Krishna Reddy, D V Kiran, B Gurappa, A Nagaraju. “Modeling simulation and analysis of pv cell boost converter fed induction motor drive with closed loop speed control”, Grenze ID: 02.CSPE.2015.4.28, Page(S): 127-136

[13]. K Krishna Reddy, N V Kishore Kumar. “A New Z-Source Multilevel Inverter for Induction Motor Drives”, IJSETR,ISSN2319-8885,Vol.04,Issue.10,April-2015, Pages:1901-1906.

[14]. K. Krishna Reddy, D V Kiran. “Torque Ripple and Harmonics Reduction in BLDC Drive using Multilevel Inverter ”, IJATIR, ISSN 2348–2370, Vol.07, Issue.03, April-2015, Pages: 0367-0373.